Stress relaxation of PBI based membrane electrode assemblies

Alexander P. Suvorov *, John Elter, Rhonda Staudt, Robert Hamm, Gregory J. Tudryn, Linda Schadler, Glenn Eisman

Department of Materials Science, Rensselaer Polytechnic Institute, Troy, NY 12180-3590, United States
Plug Power Inc., Latham, NY, United States

ABSTRACT

Stress relaxation in the membrane electrode assemblies (MEA) in PEM fuel cells subjected to compressive loads is analyzed. This behavior is important because nonzero contact stress is required to maintain low electric resistivity in the fuel cell stack. Experimental results are used to guide the choice of the viscoelastic properties of the constituents of the MEA, the membrane and the gas diffusion layer (GDL), needed for the model. These properties are incorporated into the model that treats the membrane as a porous-viscoelastic solid, and the gas diffusion layer as a nonlinear elastic solid. Using numerical simulations (finite element method), the stress relaxation curves for the MEA are obtained for different fluid flow boundary conditions, variations in the material properties of the membrane and the GDL. The results are compared to experimental stress relaxation curves. Most of the experimental data were obtained at a temperature of 180 °C, corresponding to operating conditions, so in the model the temperature was considered fixed and equal to this value.

© 2008 Elsevier Ltd. All rights reserved.

1. Introduction

The objective of this paper is to study the mechanical behavior of the polybenzimidazole (PBI) based membrane electrode assemblies (MEA) subjected to compressive loads. MEA stacks are used as a primary part of PEM fuel cells that produce electricity by means of chemical reactions. Usually the MEA is a layered material that consists of the viscoelastic membrane or gel layer and outer gas diffusion layers. Under applied compressive strains the contact stress on the surface of the MEA will drop with time due to the intrinsic relaxation of the stresses in the membrane, and the partial crushing of the GDLs. However, to maintain low resistivity of the MEA over time (years), the contact stress should be sufficiently large in the long term to maintain good electrical contact.

The purpose of this study is to show how the stress relaxation behavior in the PBI-based MEA, subjected to compressive strain, depends on the properties of the individual components of the MEA, membrane, and the GDLs. Understanding the behavior of the membrane is crucial to understanding the stress relaxation behavior in the MEA. The fact that gels exhibit significant stress relaxation in compression was observed by Guenet and McKenna (1986) and McKenna and Guenet (1988). They demonstrated that at room temperature the gels show a double logarithmic stress relaxation rate, m. The slope of the stress relaxation curve $m = -log(\sigma_R)/log(t)$ was found to be nearly a constant ($m = 0.1 - 0.15$) over the time range $t < 1000$ s for gels. However, above 1000 s the rate of stress relaxation increased, especially at low concentrations of polymer.

---

* Corresponding author. Address: Department of Materials Science, Rensselaer Polytechnic Institute, Troy, NY 12180-3590, United States. Tel.: +1 518 2717923; fax: +1 518 2768784.
  E-mail address: suvora@rpi.edu (A.P. Suvorov).

The viscoelastic behavior of gels is attributed, in part, to the frictional forces between the fiber network of the gel and the gel liquid. The viscoelastic properties of the gel were obtained by Tanaka et al. (1973) by studying the spectrum of light scattered from the viscoelastic gel. Zhang et al. (1998) proposed to use rubber elasticity theory for describing mechanical behavior of the gel. The shear modulus of the gel was found to be a nonlinear (power law) function of the polymer concentration.

The mechanical behavior of high porosity gels or aerogels was studied by Ma et al. (2002). They created a computer model of the gel network that recovers a known scaling relationship between the Young's modulus and the relative density.

In this work, the membrane or gel will be modeled as a viscoelastic porous material. A porous material was chosen because these materials can lose liquid under deformation and this fact, in part, explains stress relaxation and creep. The theory of porous solids was developed by Biot (1941), and advanced further mainly for soil mechanics applications by many researchers (Freudenthal and Spillers, 1962; Booker and Small, 1987; Rice and Cleary, 1976). Classical consolidation process of soil is considered in the book by Coussy (2004). Scherer (1989) applied the theory of poroelasticity to model the mechanical behavior of gels. A useful extension of Biot's theory which does not neglect the shear stress in the fluid is presented in the paper by Wolgemuth et al. (2004).

This paper is organized as follows. Section 2 describes the materials used in the MEA, the structure of the MEA and the fabrication procedure. Section 3 describes the geometry of the MEA and the boundary conditions for the finite element model. Sections 4 and 5 describe the material properties of the membrane and the GDL, respectively. Section 6 presents comparison of the numerical and experimental results pertaining to the stress relaxation of the entire MEA.

2. MEA structure and fabrication

The MEA consists of outer GDLs, and a relatively thin internal layer – membrane or a gel. The MEA is compressed between rigid metal plates that usually have a channel-plate configuration (Fig. 1). This assemblage is stacked with similar ones. Typically 100–200 MEAs, shown in the Fig. 1, are stacked together to form a fuel cell stack. To simplify the model, only one MEA is modeled in the present study – it is believed that this model is able to represent typical mechanical behavior of the real stack components. We distinguish two stages of the MEA operation: bonding stage (fabrication) and the postcompression stage (service). In the bonding stage, the initial membrane thickness can be equal to about 375 μm. By applying pressure at modestly elevated temperatures during the bonding, the number of air pores in the membrane and the GDL are reduced, better bonding between the GDL and the membrane is achieved. The membrane thickness can drop down to 200 μm. After that, the service load is actually applied, and the postcompression stage begins. We will be focusing mostly on the postcompression stage.

The GDL supplied by E-TEK Inc. consists of three layers. The thickest macro-porous carbon layer usually has a thickness of 290–400 μm. The middle layer is a hydrophobic micro-porous layer. Its thickness can range from 10 μm to 100 μm. The catalyst layer is the thinnest one, it has a thickness of about 30 μm. The GDL is placed such that the catalyst layer faces the membrane, and the outer macro-porous layer faces the rigid metal plates (Fig. 1). In the present study, the GDL will be modeled as a single layer imitating the combined mechanical response of all three layers. Individual properties of the layers in the GDL certainly affect its overall properties. For example, it was observed that due to the presence of the micro-porous layer, the overall permeability of the E-TEK GDL is small compared to that of other GDLs such as Toray GDL (Fenton and Kunz Research group, 2003).

The membrane or gel consists of polymer and liquid. The liquid consists of two phases: water and phosphoric acid (PA). One of the questions that can be of interest is how the liquid and polymer content in the gel changes under compressive load applied to the MEA and how much liquid in the gel is lost under compression. To answer this question we compressed the
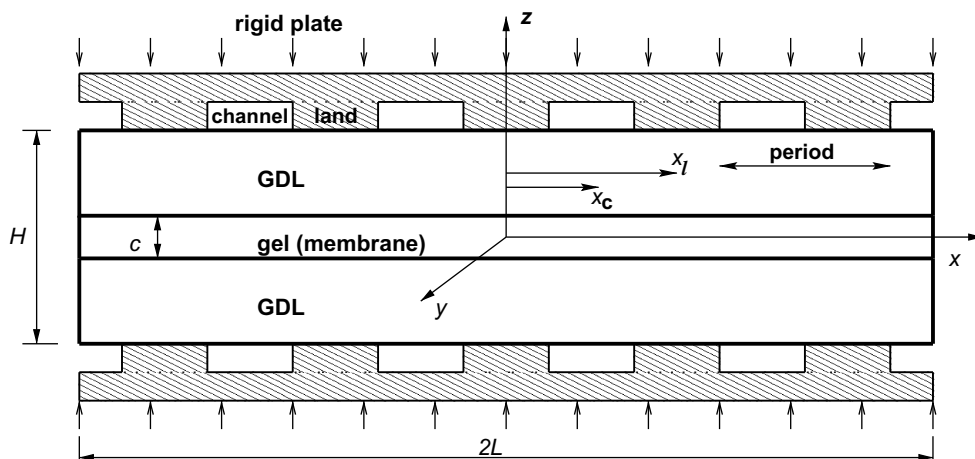

Fig. 1. Geometry of the MEA.

Table 1
Change in the composition of the membrane for the MEA compressed between the channeled plates

Membrane thickness (μm)	Polymer content (%)	Water content (%)	PA content (%)
375	5	51.1	43.9
300	5.6	43.6	50.8
250	5.4	43.8	50.8
200	7.5	44.4	48.0
150	9.1	44.8	46.1
100	12.7	39.7	47.5
75	19.4	37.8	42.7
50	29.1	42.9	28.1

Initial membrane thickness 375 μm.

MEA supplied by industry between the channeled plates, Fig. 1, as it was done in real fuel cells. After applying the compressive load, the MEA was split along the interface with a sharp instrument and the contents and the thicknesses of each layer were measured. In particular, we weighed the sample, titrated it to determine the acid content, then the acid and all liquids were removed from the membrane by an acid washing followed by a drying step. The membrane was then reweighed to determine the polymer content.

It was found that the weight percent of the polymer in the fresh, not compressed, PBI membrane is very small, equal to about 5%, thus most of the volume in the membrane is taken by the liquid (Table 1). In the fresh membrane the weight percent of the phosphoric acid is approximately equal to that of the water. If the fresh membrane is compressed, the weight percent of the liquid drops, however, the change in the weight percent was observed to be insignificant at the initial stages of compression. In particular, during compression, as the thickness of the membrane changes from 375 μm (fresh membrane) to 150 μm, the weight percent of the polymer changes from 5% to 9%. The weight percent of the liquid decreased by 4%. This suggests that the fresh membrane has a certain amount of void volume, and it is partially saturated with liquid.

In the postcompression stage or, equivalently, under service conditions, the membrane thickness is reduced from 200 μm to lower values, but in the range 200–100 μm, according to experimental data, the polymer content remains low, approximately equal to 5–12% (Table 1). The membrane does not lose much liquid at this stage. Deformation of the solid part of the gel, skeleton, can be explained by further compaction of the air pores and liquid motion to less stressed areas of the membrane. Further compression of the membrane down to a thickness 50 μm caused a more rapid increase in the weight percent of the polymer up to 29%. The weight percent of the liquid is reduced by 24%. Now the change in the weight percentages is primarily attributed to the escape of the liquid during compression. However, it appears that the liquid can escape here under constantly increasing compressive loading applied to the MEA. In the postcompression stage, however, when the membrane becomes thinner than 100 μm, the local stress in the membrane is low due to preceding relaxation and can hardly cause further compression of the membrane, and subsequently, the reduction of the liquid content. It was difficult to compress the membrane below a thickness of 50 μm. No significant changes in weight percentage of the liquid or polymer were observed in this range. This can be explained by the low permeability of the thin membranes, i.e., perhaps by the closed structure of their pores.

In service, the temperature is increased to $\approx$180 °C, and afterwards the compressive load is gradually applied to the fuel cell stack. Measurements of the GDL and membrane properties are also done at 180 °C. In the model, we assume that the temperature is kept fixed and equal to the operating temperature at all time. All properties are considered to be independent of the temperature.

3. Geometry and boundary conditions

Consider one single MEA (membrane electrode assembly) compressed between channeled plates (Fig. 1). The geometry of the structure does not change along the y-axis, therefore, the only crossection of the structure shown on the figure is in the xz plane. The plates or coupons are made of metal, and thus are very rigid compared to the compliant MEA. The plates have a typical land and channel configuration, as shown on the figure, with lands in contact with the GDLs.

The uniform displacement w^0 is prescribed on the outer surfaces of the plates which results in the compressive strain within the MEA evaluated as

$$\epsilon_z^0 = \frac{(H - 2w^0) - H}{H} = -\frac{2w^0}{H} \tag{1}$$

Table 2
Geometry of the fabricated MEA

Total thickness, H (mm)	1.016
Membrane thickness, c (mm)	0.2032
Channel width (mm)	1
Land width (mm)	1

where H is the height of the MEA (Table 2). Deformation of the plates was not included in (1) because of their high rigidity. Therefore, vertical displacement at the zones of contact between the coupons and the GDL was also assumed to be equal to w^0. The boundary conditions at the upper surface of the GDLs are

$$
\begin{aligned}
w(x_l, H/2) &= -w^0, & \sigma_{xz}(x_l, H/2) &= 0 \\
\sigma_{zz}(x_c, H/2) &= 0, & \sigma_{xz}(x_c, H/2) &= 0
\end{aligned}
\tag{2}
$$

where x_l pertains to the land area, and x_c to the channel area. Friction between the coupons and the GDL was neglected since the surface of contact was assumed smooth.

Due to the symmetry of the problem with respect to the x-axis, it is sufficient to model only the upper half of the MEA, i.e., $z \geqslant 0$. The symmetry boundary conditions at $z = 0$ are

$$
w(x, 0) = 0, \qquad \sigma_{xz}(x, 0) = 0
\tag{3}
$$

The number of the lands or channels in the x-axis direction can be quite large, and the total length of the structure along the x-axis $2L$ is much larger than the thickness H. The width of the structure $2B$ is also large compared to the thickness H but can be smaller than the length $2L$. The edges $x = \pm L$, $y = \pm B$ are traction free:

$$
\begin{aligned}
\sigma_{xx} &= \sigma_{xy} = \sigma_{xz} = 0, & x = \pm L \\
\sigma_{yy} &= \sigma_{yx} = \sigma_{yz} = 0, & y = \pm B
\end{aligned}
\tag{4}
$$

In view of the boundary conditions (2), (3) and invariance of the geometry along the y-axis, it is clear that the most significant deformation occurs in the xz plane.

To reduce computational effort, this problem can be treated as a 2D plane strain problem assuming that instead of the traction free boundary condition $\sigma_{yy} = 0$ at $y = \pm B$, the strain $\epsilon_y = 0$. This can cause some error in the results but allows consideration of a 2D plane strain problem instead of 3D problem with $\epsilon_y \neq 0$. Numerical tests showed that the error introduced due to this assumption is not large, approximately equal to 10%.

If this problem is solved by one of the numerical methods such as a finite element method, another simplification can be gained by reducing the number of channels or lands along the x-axis, i.e., by shortening the model. Instead of (4)$_1$ one can consider a constrained edge $x = \pm L$, i.e., and prescribe the overall strain $\epsilon_x = 0$ by setting

$$
u(\pm L, z) = 0, \qquad \sigma_{xz} = \sigma_{xy} = 0, \quad x = \pm L
\tag{5}
$$

Then, due to periodicity of the structure, it is enough to model only one land and one channel and prescribe (5) at the edges of the model. This will result in the shortest model. However, additional constraining of the model along the x-axis will lead to significant errors, especially in a problem with incompressible constituents. In particular, when the displacement, w_0, is prescribed as in (2), by constraining the edges (5), one can elevate the stresses σ_z in the structure, as compared to the stresses in the real structure with traction free edges. Therefore, the boundary conditions (4)$_1$ at the edges $x = \pm L$ were retained, i.e., left free of tractions.

The number of the channels or lands that should be retained in the finite element model with free edges $x = \pm L$ is also of concern. Our numerical tests showed that the results are not affected by increasing the length of the structure beyond that of five to six channels or lands. Due to the symmetry of the problem with respect to the z-axis, the number of channels or lands can be reduced roughly to 3, and the symmetry boundary conditions at the center $x = 0$ must be

$$
u(0, z) = 0, \qquad \sigma_{xz} = 0
\tag{6}
$$

Since the present problem is rate-dependent, the applied displacement w^0 is assumed to be a function of time. In the stress relaxation test, w^0 is theoretically defined as

$$
w^0(t) = w^0_{max}\theta(t)
\tag{7}
$$

where $\theta(t)$ is a step function, i.e., the function which is zero at $t < 0$ and equal to 1 at $t > 0$, w^0_{max} is the maximum displacement applied. In practice, though, the change from zero displacement to the maximum does not happen instantaneously but takes a certain amount of time, usually 0.5-1 min. Therefore, w^0 can be taken as

$$
\begin{aligned}
w^0(t) &= \frac{w^0_{max}}{t_1}t, & 0 < t < t_1 \\
w^0(t) &= w^0_{max}, & t > t_1
\end{aligned}
\tag{8}
$$

If the model includes poroelastic materials, one needs to prescribe the conditions for the fluid flow at the boundary of the model. In the present study, the gel is assumed to be a poroelastic material, and the GDL is an elastic material. Thus, fluid flow conditions need to be prescribed at the boundary of the gel. Due to the symmetry of the model it is clear that

$$
\begin{aligned}
v_x(0, z) &= 0, & 0 \leqslant z \leqslant c/2 \\
v_z(x, 0) &= 0
\end{aligned}
\tag{9}
$$

where v_x, v_z are the x and z components of the fluid velocity, respectively. At the right edge of the membrane, zero pressure is prescribed since this edge is free, i.e.

$$p(L/2, z) = 0, \quad 0 \leqslant z \leqslant c/2 \tag{10}$$

At the GDL/membrane interface, the velocity can be prescribed as a linear function of the pressure

$$v_z(x, c/2) = Kp(x, c/2) \tag{11}$$

where p is the pressure, and K is a coefficient of proportionality. When $K = 0$, the velocity is zero and thus the interface is insulating in terms of the fluid motion. If K is large, then the pressure on the interface must be small in order to keep the velocity finite. This means that when K is large, the interface is perfectly conducting. Of course, the value of the coefficient K is related to the structure of the GDL and the size of its pores. The exact relationship was not established.

It is assumed that in the membrane electrode assembly the GDLs are perfectly bonded to the membrane (gel), and thus on the interface the stresses and displacements are continuous

$$\begin{aligned} \sigma_z^{(1)}(x, c/2) &= \sigma_z^{(2)}(x, c/2), \quad \sigma_{xz}^{(1)}(x, c/2) = \sigma_{xz}^{(2)}(x, c/2) \\ u^{(1)}(x, c/2) &= u^{(2)}(x, c/2), \quad w^{(1)}(x, c/2) = w^{(2)}(x, c/2) \end{aligned} \tag{12}$$

where the index 1 or 2 refer to the layer number, 1 for the GDL layer, and 2 for the membrane. c is the total thickness of the membrane.

Finally, the average contact stress is defined. The distribution of the compressive stress σ_z along the length of the structure will be nonuniform, with the maximum under the lands, and the minimum in the channel areas. Therefore, to characterize the mechanical response of the structure, in particular, the stress relaxation behavior, the average contact stress, or simply the contact stress, is defined as follows:

$$\sigma_z^c = \frac{1}{2L} \int_{-L}^{L} \sigma_z(x, z) \mathrm{d}x \tag{13}$$

Because of the force equilibrium, the value of the coordinate z in (13) should not affect the value of the contact stress. Thus, either the stress in the GDL material or the membrane can be used for evaluation of the average contact stress.

4. Membrane (gel) constitutive equations

In the present paper the membrane layer is modeled as a nonlinear porous-viscoelastic material. As a poroelastic material, the gel is being viewed as a skeleton, pores of which are filled with liquid. The gel is assumed to be fully saturated with liquid at all times but perhaps initially when some of the air pores may be present. We did not attempt to model the gel as a partially saturated solid with low, smaller than 0.9, value of the saturation. The model of a partially saturated membrane in that case turned out to be prohibitively complex and perhaps unjustified for the case of the postcompression loading.

As it follows from Table 1, in the range of the membrane thicknesses 375–100 μm, the polymer weight percent does not change significantly. We set the initial solid content equal to 5%. When the membrane becomes thinner than 100 μm, due to the preceding relaxation, the compressive stress gets low and can hardly lead to further compression of the membrane, and subsequently, to the liquid loss and the increase in the polymer content. Anyway, it is known that the polymer content remains low for all time, and it was suggested by preliminary numerical results that the exact number is unimportant. The solid material of the skeleton can fill an insignificant volume compared to the volume of the pores or liquid inside. However, due to its structure, the skeleton may support an appreciable amount of stress.

The total stresses in the porous material are obtained by the superposition of the stresses in the skeleton and the pressure in the liquid, p. It is assumed that $p > 0$ for totally saturated solids, and $p < 0$ for partially saturated solids. Thus, the total stress is

$$\sigma_{ij} = \sigma_{ij}^s - \alpha p \delta_{ij} \tag{14}$$

where the index s indicates that this is the stress in the skeleton. Parameter α is equal to 1 for solids totally saturated with liquid, $\alpha < 1$ for partially saturated solids. As it is seen from (14), the liquid supports only normal stresses in the present formulation.

Consider first the constitutive equations for the linear poroelastic solid formulated first by Biot (1941). For the 2D deformation in xz plane the stress–strain relation can be written as

$$\begin{aligned} \sigma_x^s &= 2G\left(\epsilon_x + \frac{\lambda}{2G}\epsilon\right) \\ \sigma_z^s &= 2G\left(\epsilon_z + \frac{\lambda}{2G}\epsilon\right) \\ \tau_{xz}^s &= G\gamma_{xz} \end{aligned} \tag{15}$$

where σ_{ij}^s is the stress in the drained skeleton, λ and G are the elastic moduli of the skeleton, ϵ_{ij} is the strain, defined in terms of the displacements u_i as follows:

$$\epsilon_{ij} = \frac{1}{2}(u_{i,j} + u_{j,i}) \tag{16}$$

and

$$\gamma_{xz} = 2\epsilon_{xz}, \quad \epsilon = \epsilon_x + \epsilon_y + \epsilon_z, \quad \epsilon_y = 0 \tag{17}$$

In the present study, the skeleton of the membrane is modeled as a nonlinear elastic material by using the elastomeric foam model available in the finite element program ABAQUS. The strain energy for an elastomeric foam under isothermal conditions is given by

$$U = \sum_{i=1}^{N} \frac{2\mu_i}{\alpha_i^2}[\lambda_1^{\alpha_i} + \lambda_2^{\alpha_i} + \lambda_3^{\alpha_i} - 3 + \frac{1}{\beta_i}((\lambda_1\lambda_2\lambda_3)^{-\alpha_i\beta_i} - 1)] \tag{18}$$

where λ_i are the principal stretches, N, μ_i, α_i, β_i are material parameters. The coefficients μ_i are related to the shear modulus, μ_0, by

$$\mu_0 = \sum_{i=1}^{N} \mu_i \tag{19}$$

The coefficient β_i determines the degree of compressibility. β_i is related to the Poisson's ratio, v_i, by the expression

$$\beta_i = \frac{v_i}{1 - 2v_i} \tag{20}$$

The bulk modulus K_0 follows from:

$$K_0 = \sum_{i=1}^{N} 2\mu_i\left(\frac{1}{3} + \beta_i\right) \tag{21}$$

Table 3 gives several combinations of materials parameters for the membrane's skeleton used in the present study. N, the number of terms in the sum, was set equal to 3 to represent complex nonlinear behavior of the gel. The properties given in the table pertain to the initial, i.e., instantaneous response of the membrane, as opposed to the long term response, which is important for the viscoelastic solids. For the viscoelastic material, such as the gel, the constitutive equations must also reflect the dependence of the elastic moduli on time. It is assumed that the coefficient μ_i is a function of time, and it is taken in the form of a Prony's series

$$\mu_i(t) = \mu_i^0\left(1 - \sum_{k=1}^{M} r_k\left(1 - \exp\left(-\frac{t}{\beta_k}\right)\right)\right) \tag{22}$$

where μ_i^0 is the initial shear modulus of the skeleton, denoted in (19) by μ_i, r_k and β_k are material constants. For most of the cases, it was found that in order to match the experimental data it was sufficient to keep just one term in the series expansion (22), i.e. $M = 1$. The properties are listed in Table 3.

Another part of the constitutive equations relates to the fluid motion inside the porous solid. For a totally saturated solid with incompressible constituents, the change in the liquid content, θ, is equal to the volumetric strain, ϵ, defined in (17). Conservation of mass implies that divergence of the velocity of the fluid must be equal to the rate of change in the liquid content with a minus sign, i.e.

$$\frac{\partial\theta}{\partial t} = -v_{x,x} - v_{z,z} \tag{23}$$

where v_x, v_z are components of the velocity vector of the fluid.

Another equation, Darcy's law, states that the velocity of the fluid is related to the pressure gradient as

$$v_x = -k_r\frac{k_x}{\mu}p_{,x}, \qquad v_z = -k_r\frac{k_z}{\mu}p_{,z} \tag{24}$$

Table 3
Material properties of the membrane

Set	μ_1 (MPa)	α_1	μ_2 (MPa)	α_2	μ_3 (MPa)	α_3	v_i	r_1	β_1 (s)	k (mm^2)	s_0
A	0.11	6.0	0.44	8	0.14	18	0.1	0.95	14	1.544e^{-14}	0.9
B	0.09	6.0	0.15	10	0.04	16	0.1	0.96	14	1.544e^{-14}	1
C	0.1	8.0	0.16	12	0.025	16	0.1	0.92	20	1.544e^{-12}	1

Conversion to psi: psi = MPa $\times$ 1000/6.89, MPa = N/mm^2.

where μ is the fluid viscosity, k_x, k_z are absolute permeabilities of the solid skeleton to the fluid motion in x and z directions, respectively, k_r is the relative permeability. Here, it is assumed that $k_x = k_z = k$. The relative permeability k_r is usually taken as a function of saturation s, $k_r = s^3$, which is equal to 1 for the totally saturated solid, $s = 1$. The viscosity of the fluid was taken equal to that of phosphoric acid $\mu = 3.86\,e^{-9}$ MPa s. The value of the absolute permeability is given in Table 3. To determine the viscoelastic parameters for the skeleton of the gel, and the permeability, results of numerical simulation were matched with the available experimental data. During the experiment a relaxation test was performed in which the gel alone was compressed between the channeled plates, similar to those shown in Fig. 1. The maximum value of compressive strain was equal to 0.25, the duration of loading was $t_1 = 48$ s, which gives a rate of loading equal to 0.0052 s^{-1}. The experimental stress relaxation curve is shown with a dashed line in Fig. 2, and the experimental stress–strain curve is shown in Fig. 3.

In the finite element model of the membrane the boundary conditions were taken to be identical to those given by (1)–(4), (6), (8), (9), (10) with the total height, H, of the MEA in (1), (2) now replaced by the thickness of the gel, c. At the upper surface of the membrane $z = c/2$, zero pressure was prescribed in the channeled areas, and zero velocity in the land areas

$$v_z(x_l, c/2) = 0, \qquad p(x_c, c/2) = 0 \tag{25}$$

where the coordinate x_l refers to the lands, x_c to the channel.

The experimental stress relaxation curve for the gel is shown in Fig. 2 with the dashed line, and the average contact stress obtained numerically is shown with a solid line. The material parameters set A (Table 3) was used to show the numerical results in the figure. Other combinations of parameters did not produce significant changes in the stress relaxation curve. Initial saturation s for set A was taken equal to 0.9, but quickly changed to 1 due to applied compression and low permeability. Note that in order to model the solid with saturation smaller than 1, the dependence of the liquid pressure on saturation, s, for $s < 1$ must be prescribed. It was assumed that as the saturation of the partially saturated membrane changes from 0.9 to 0.999 the liquid pressure can change from -0.01 MPa to 0 MPa. Note that the liquid pressure is negative for a partially saturated membrane, which is due to surface tension. (Small value for the liquid pressure as opposed to larger ones does not significantly affect the value of the overall stress and reduces the computational effort; therefore, it was chosen to be small. Moreover, the liquid pressure at such large values of saturation should approach zero and cannot be large.)

It is clear that under compression the membrane shows a high rate of stress relaxation, and low value of stresses in the long term compared to the maximum stress at time $t = t_1$. The relaxation of stresses in the membrane can be due to the following factors (a) ability of the membrane to lose liquid, (b) intrinsic viscoelastic behavior of the skeleton, (c) relaxation of the shear stresses in the fluid. The factor (c) can be eliminated if the rate of loading is not too high, which allows the shear stresses in the fluid to be neglected. To find out which factor (a) or (b) explains the significant stress relaxation, assume first that the absolute permeability k is small. In this case, the stress supported by the fluid, namely pressure, can be large, once the membrane reaches its totally saturated state. If the skeleton were elastic, not viscous, the relaxation would take place at a very low speed since the permeability is small. But from the experimental data it is obvious that the relaxation is rapid and significant, thus, the skeleton is viscoelastic with small relaxation time β_1, see (22). Suppose now that the permeability k is large. The fluid then can escape easily through the gel boundaries. Since the rate of loading is quite slow, namely 0.0052 s^{-1}, owing to the large permeability k, the fluid will not support a significant amount of stress, i.e., the fluid pressure will be
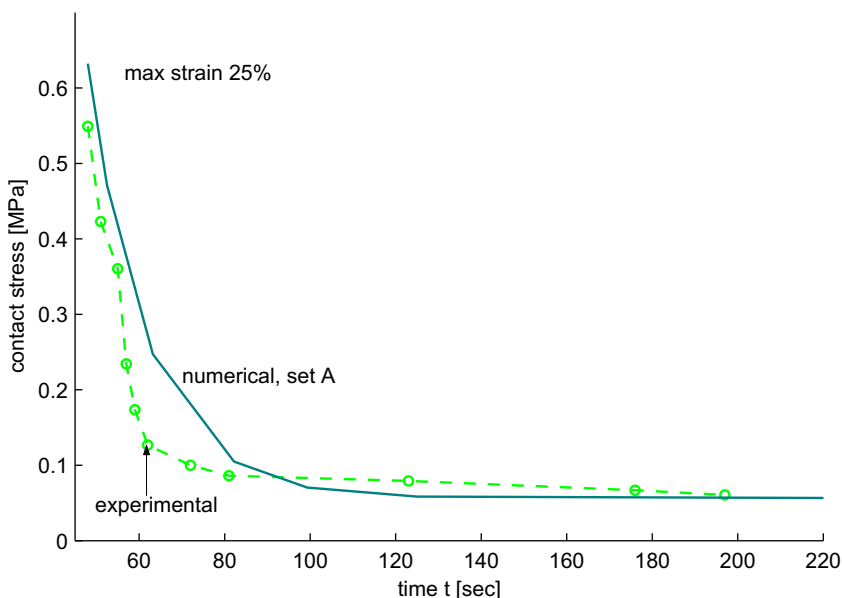

Fig. 2. Stress relaxation test for the membrane (gel) compressed between the channeled plates; maximum strain is 0.25.
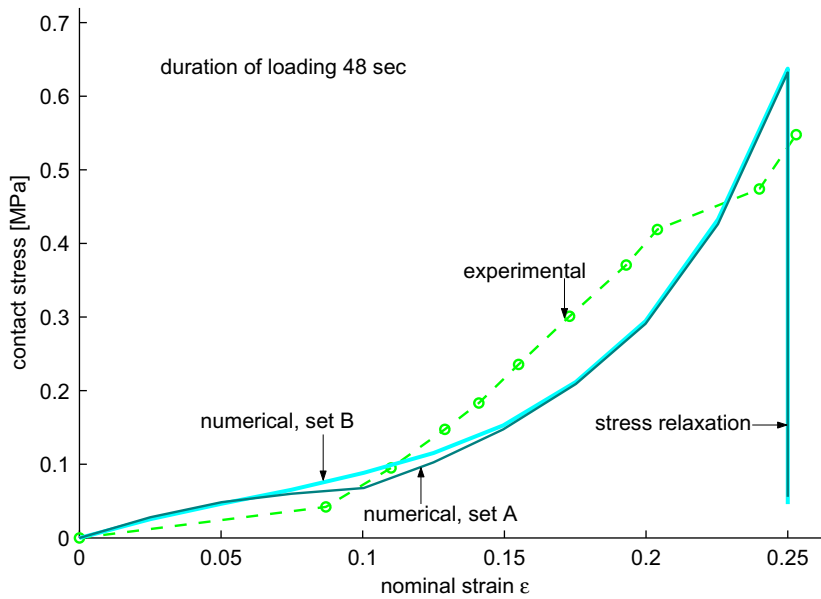
Fig. 3. Stress–strain curve for the gel (membrane) compressed between the channeled plates during loading from zero strain to the maximum value 0.25.

small. Thus, the stress will be mainly supported by the skeleton that must be initially stiff to support the high stress (about 0.65 MPa on Fig. 3) when the loading has just been completed. The subsequent stress relaxation, however, is rapid and significant, so the skeleton must be again viscoelastic with small relaxation time, β_1. Thus, in both cases, large and rapid relaxation of the stress in the membrane occurs because of the viscoelastic behavior of the skeleton.

During loading $0 \leqslant t \leqslant t_1$ the gel behaves like a nonlinear elastic material, Fig. 3. The elastic modulus of the skeleton μ_0, and the exponents α_i must be sufficiently high so that the maximum stress can be reached at the time $t = t_1$ when the maximum strain is attained. This figure presents the results for the material parameters sets A and B, Table 3. The only difference is that the stress–strain curve for the set A has a corner corresponding to the strain at which the membrane becomes totally saturated. The curve for set C is not shown since it is similar to that for the parameters set B.

We admit that the match between the numerical and experimental results is not exact especially at the loading stage. It was not clear to us if it is possible to obtain a better match by using the constitutive law (18) or by using another nonlinear model. However, it turned out that the relaxation part of the constitutive behavior of the gel is more important, and even by using a linear viscoelastic model a tolerable agreement can be obtained when it comes to the stress relaxation behavior, Fig. 2.

5. GDL constitutive equations

Strictly speaking, the GDL material is also a poroelastic material, but the pores are only partially saturated with the fluid and an appreciable fraction of pores remain filled with air. In partially saturated solids, the pressure of the fluid can be assumed to be small compared with the stresses in the skeleton, solid part, and the GDL can be reasonably well modeled as an elastic solid by ignoring the pressure in the fluid. It was also observed that the GDL is not strongly rate dependent, therefore viscous effects in the GDL skeleton were also neglected.

The GDL was modeled as a hyperelastic material with the strain energy taken in Ogden form, which is for the isothermal condition is given by the expression similar to (18)

$$U = \sum_{i=1}^{N} \frac{2\mu_i}{\alpha_i^2}(\bar{\lambda}_1^{\alpha_i} + \bar{\lambda}_2^{\alpha_i} + \bar{\lambda}_3^{\alpha_i} - 3) + \sum_{i=1}^{N} \frac{1}{D_i}(J - 1)^{2i}, \quad J = \lambda_1 \lambda_2 \lambda_3 \tag{26}$$

where $\bar{\lambda}_i = J^{-1/3}\lambda_i$ are the deviatoric stretches, λ_i are the principal stretches, N, μ_i, α_i, and D_i are the material parameters, related to the shear modulus μ_0 and bulk modulus K_0 of the material as follows:

$$\mu_0 = \sum_{i=1}^{N} \mu_i, \qquad K_0 = \frac{2}{D_1} \tag{27}$$

Specific values of the material parameters for the gas diffusion layer studied in this paper are shown in Table 4. They are obtained by comparing results of numerical calculation with the experimental data. During the experiment, the GDL alone

Table 4
Material properties of the GDL

Set	μ_1 (MPa)	α_1	D_1 (1/MPa)	r	m (N mm)	β
I	1.1	35	2.64	1.03	0.004	0.018

was compressed between the channeled plates of Fig. 1. A reasonably good agreement was found when N was taken equal to 1; the elastic parameters μ_1, D_1, given in the table, were calculated by assuming that the Poisson's ratio $v = 0.01$.

It was observed that under compression, the behavior of the GDL during initial loading is different from the unloading–reloading behavior. The softening of the GDL during the unloading is associated with the damage of the material caused by compression. To take into account this difference in the elastic moduli during the loading and unloading, the Mullins effect model was used. As indicated in the ABAQUS user manual, this model originally was developed to model stress softening of filled rubber elastomers under quasi-static cyclic loading.

The strain energy for a material exhibiting the Mullins effect is given by

$$U = \eta \widetilde{U}_{\text{dev}}(\bar{\lambda}_i) + \widetilde{U}_{\text{vol}}(J) \tag{28}$$

where $\widetilde{U}_{\text{dev}}$ and $\widetilde{U}_{\text{vol}}$ are the deviatoric and volumetric parts of the primary strain energy, given by (26). The deviatoric part is represented by the first term on the right of (26), and the volumetric part is represented by the second term on the right side of (26). The parameter η is the damage parameter, $0 < \eta \leqslant 1$, $\eta = 1$ in the absence of damage. When the deformation of the material is on a point of the stress–strain curve that represents the primary hyperelastic behavior (loading), the damage parameter $\eta = 1$, and the strain energy (28) is reduced to the strain energy of the primary hyperelastic material (26).

The damage parameter η, varies with deformation according to

$$\eta = 1 - \frac{1}{r}\text{erf}\left(\frac{U_{\text{dev}}^{\text{m}} - \widetilde{U}_{\text{dev}}}{m + \beta U_{\text{dev}}^{\text{m}}}\right) \tag{29}$$

where $U_{\text{dev}}^{\text{m}}$ is the maximum value of $\widetilde{U}_{\text{dev}}$ during deformation history, r, β, m are material parameters, erf is the error function defined as

$$\text{erf}(x) = \frac{2}{\sqrt{\pi}} \int_0^x \exp(-w^2)\,dw \tag{30}$$

When the deviatoric part of the primary strain energy attains its maximum, $\widetilde{U}_{\text{dev}} = U_{\text{dev}}^{\text{m}}$, it is clear from (29) and (30) that $\eta = 1$, and the strain energy is equal to that of the primary hyperelastic material. On the other hand, when $\widetilde{U}_{\text{dev}} < U_{\text{dev}}^{\text{m}}$, which occurs during unloading/reloading, the damage parameter $\eta < 1$. The specific values of the material parameters chosen for the GDL are indicated in Table 4.
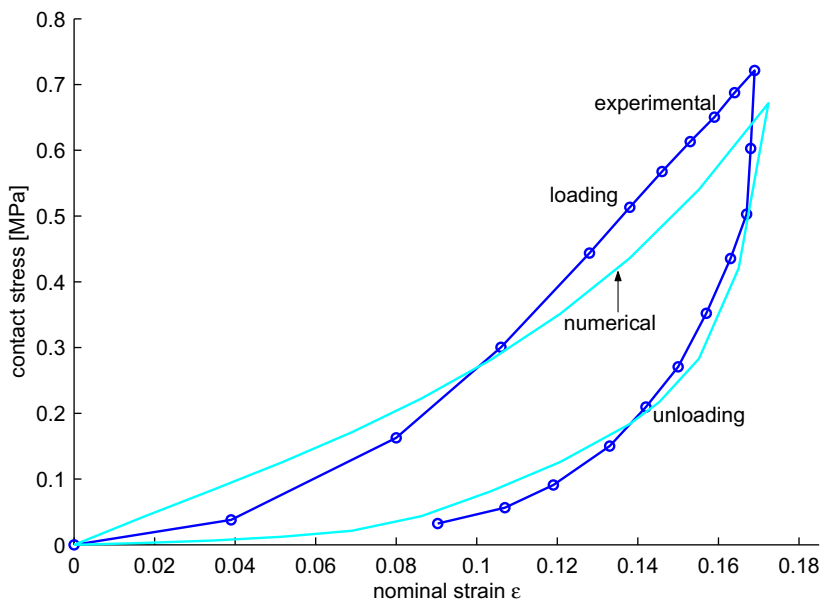

Fig. 4. Mechanical response of the hotpressed GDL in the compression test; GDL is compressed between the channeled plates.

The experimental stress–strain curve for the hot-pressed GDL material during a compression test is shown in Fig. 4 by a circled line. The increase in modulus during loading can be attributed to the compaction of the GDL pores, which results in the stiffening of the material. The hysteresis can be explained by the damage of the pores during compaction, and the irreversible deformation, which results in lower values of the elastic moduli during unloading. Only the hotpressed GDL is modeled, since it is used in actual MEA stacks. The fresh GDL, which was not hotpressed, shows softer behavior.

It is worth noting that during stress relaxation of the entire MEA, the GDL material is actually in a state of unloading, which makes the GDL stiffness at unloading an important parameter. Nevertheless, the maximum value of the contact stress in the MEA depends on the GDL stiffness during loading.

6. Stress relaxation of the MEA

With the properties of the MEA constituents, the membrane and the GDLs established, the stress relaxation behavior of the entire assembly can be modeled.

The maximum compressive strain ϵ_z applied to the MEA was 0.15. The duration of loading was equal to 48 s which resulted in a relatively slow strain rate of 0.0031 s^{-1}. The model included only three channels or lands at $x > 0$. The boundary conditions are given in (1), (2), (3), (4), (6), (8), (9), (10) and (11). During relaxation of the MEA, the displacement of the membrane tends to grow, as shown in Fig. 5. Due to approximately periodic distributions of the displacement and stress, only the results for $0 \leqslant x \leqslant 1$ mm are shown. The displacements are shown at time $t = 48$ s, at which the maximum value of the average contact stress is reached, and at very large value of time. It is clear that at small time, the displacement at the GDL/membrane interface is relatively small due to the high incompressibility of the membrane filled with liquid. In the long term, however, the compressive strains in the membrane are high due to the creep of the membrane's skeleton, and liquid motion inside the membrane. Because of the bonding between the membrane and the gas diffusion layer, the GDL will increase its thickness with time, but the membrane will become thinner. Thus, initially high compressive strains in the GDL will decrease in the long term, and consequently, the stress in the MEA will decrease. The stress distribution in the GDL for small and large time is shown in Fig. 6 for the height $z = 0.44H$, i.e., close to the outer surface of the GDL, and for $z = c/2 \approx 0.1H$, i.e. at the interface line. It is seen that the distribution of the stress is such that it is maximum in the land area and minimum in the channel area. Also, the high value of the stress at $t = 48$ s at the land's edge is due to an existing stress singularity in the contact area. In the results of Figs. 5 and 6 the gel material A and the GDL with the Mullins effect were used. The interface GDL/membrane was assumed to be hardly permeable for the liquid, and the coefficient K in (11) was set equal to a small number 1.5e−7 mm/(s MPa).

Fig. 7 shows the numerical and experimental stress relaxation curves for the MEA subjected to compressive strain 0.15. The experimental results are shown with dashed lines, numerical – with the solid lines. The membranes with material parameters in the sets A,B and C were used, Table 3, for numerical analysis. The coefficient K in (11) is taken to be 1.5e−7 mm/(s MPa), which is a small number. Thus, the interface GDL/membrane was almost perfectly insulating, and in the course of compression most of the fluid from the membrane was moving from the stressed land areas to the channel areas.
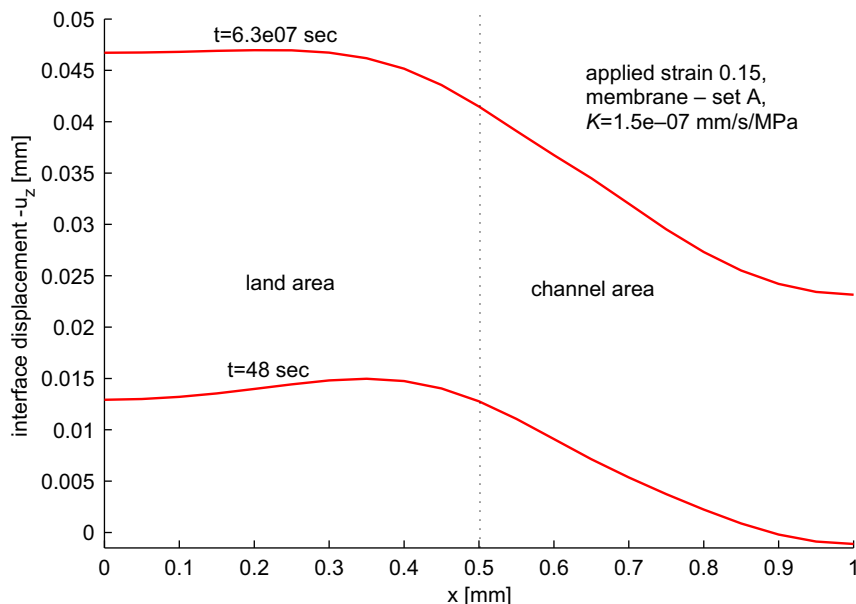

Fig. 5. Displacement distribution at the GDL/membrane interface at $z = c/2$ for the MEA subjected to compressive strain 0.15.
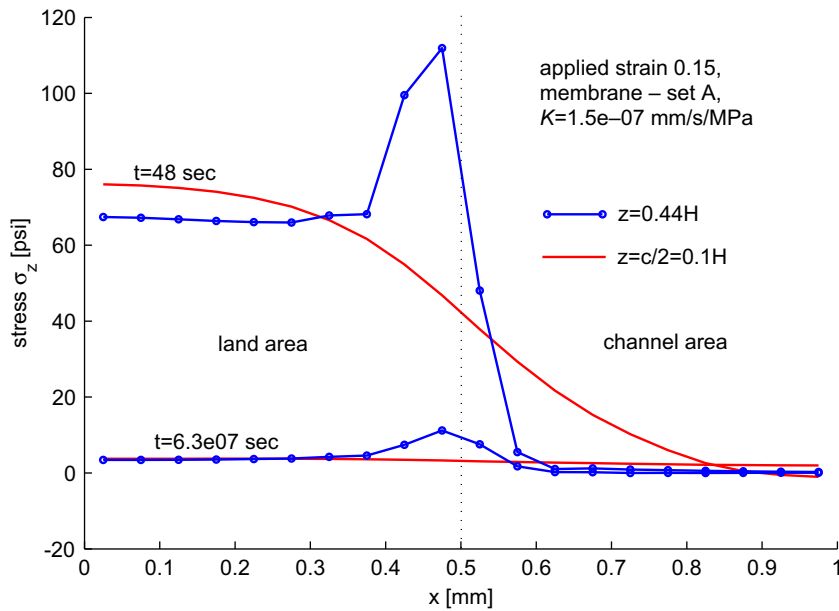
Fig. 6. Stress distribution inside the GDL at $z = c/2$ and at $z = 0.44H$ for the MEA subjected to compressive strain 0.15.
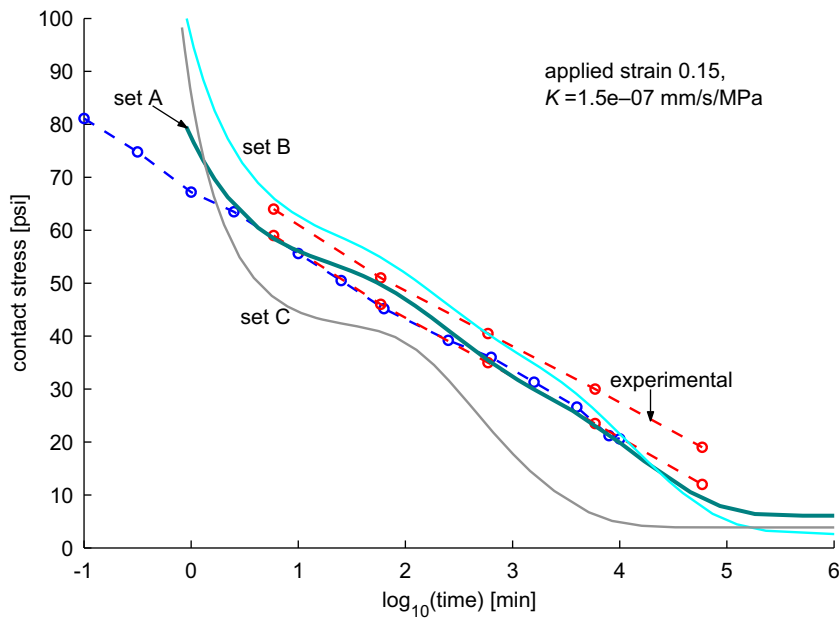

Fig. 7. Stress relaxation of the MEA with different membranes (gels); the MEA subjected to compressive strain 0.15 is compressed between the channeled plates.

It can be seen that the membrane models B and C, with initial saturations in the membrane s_0 equal to 1, give elevated values of the contact stress in the short term. This can be explained by the fact that if the membrane is initially totally saturated with liquid, the membrane is stiffer and the local strains in the membrane are smaller, which leads to an increase in the contact stress. If the initial saturation is set equal to 0.9, like in model A, the membrane is experiencing a moderate initial compression during the loading of the MEA, see Fig. 5, and the contact stress in the short term is decreased. As it was mentioned, the saturation of the membrane A changes from 0.9 to 1 in the course of the compression for $0 < t < 48$ s.

Fig. 7 shows also that the stress relaxation of the MEA with the membrane C, has a higher rate, which is not in agreement with the experimental data. Thus, the permeability of the membrane in model C is not sufficiently low to match experimental data for the MEA, even though the membrane C has similar relaxation curve to the membranes A, and B in Fig. 2.

Fig. 8 shows the stress relaxation of the MEA for two gas diffusion layers, the first one – with the Mullins effect, like in Fig. 4, and the second GDL with identical loading/unloading behavior, i.e., without Mullins effect. The properties of the gas diffusion layers are shown in Table 4. It is clear that the modulus of the GDL upon unloading has a direct impact on the rate of the stress relaxation of the MEA – the higher the modulus of the GDL, the slower the rate of the stress relaxation. Also, the ultimate contact stress is affected by the modulus of the GDL upon unloading – the higher the modulus of the GDL, the larger the contact stress. The coefficient K in (11) is taken to be equal 1.5e–7 mm/(s MPa), the same number as in Fig. 7.

Note that if the GDL/membrane interface is rather impermeable and the membrane's skeleton itself has low permeability to fluid flow, the initial drop of the contact stress in the MEA can be explained by the rapid decrease in the modulus of the
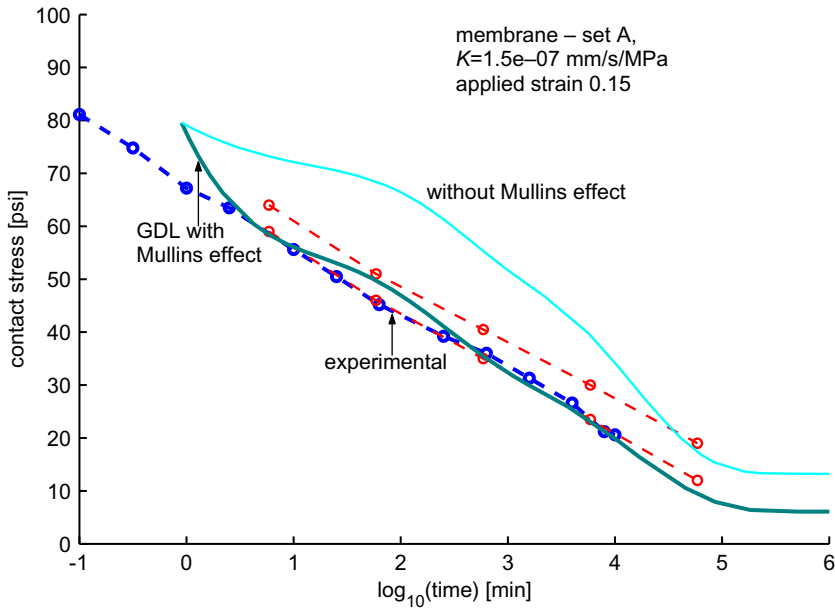

Fig. 8. Stress relaxation of the MEA with the GDL showing the Mullins effect and without Mullins effect; the MEA subjected to compressive strain 0.15 is compressed between the channeled plates.
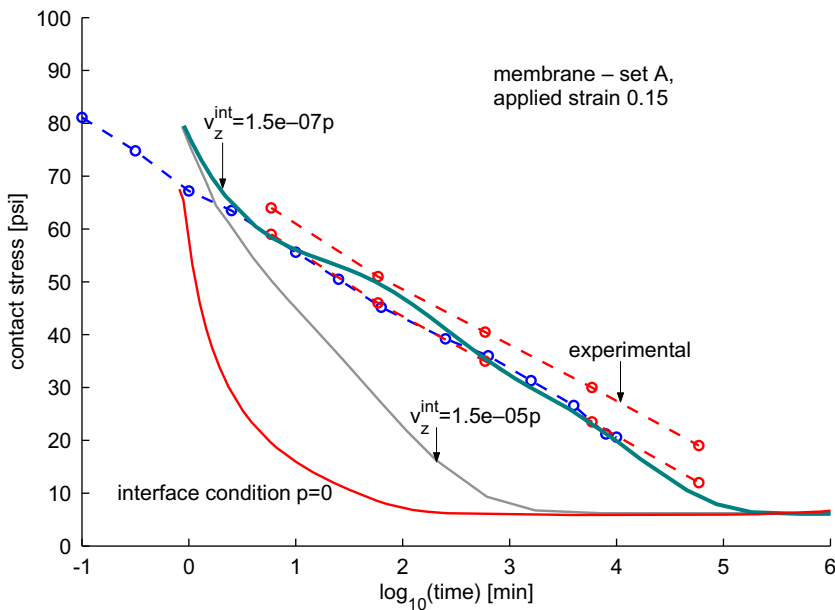

Fig. 9. Dependence of the stress relaxation of the MEA subjected to compressive strain 0.15 on the fluid flow conditions at the GDL/membrane interface; the MEA is compressed between the channeled plates.

GDL upon unloading, Fig. 4. In fact, even small local compressive strain existing in the membrane initially, see Fig. 5, will lead to the large reduction in the overall stress if the GDL is soft at unloading. Thus, in the short term there is little contribution to the overall stress relaxation caused by the membrane. In the long term, however, the behavior the MEA is controlled both by the viscoelastic behavior of the membrane's skeleton and the value of the stiffness of the gas diffusion layer upon unloading. And, in particular, the ultimate (minimum) value of the contact stress in the MEA will depend on the ultimate value of the contact stress supported by the membrane in the stress relaxation test, Fig. 2. Fig. 9 shows the stress relaxation curves for different values of the parameter K in (11). It is clear that when the pressure p is small or the fluid velocity is large across the GDL/membrane interface, the rate of the stress relaxation of the MEA will be high due to liquid loss from the membrane across the interface. The ultimate value of the contact stress is independent of K, however.

It is important here to contrast the boundary conditions corresponding to the open edges $x = \pm L$ and the closed edges, i.e., $(4)_1$ and (5). All results presented so far correspond to the open edges. The boundary condition $(4)_1$ implies that the overall stress in the direction of the x-axis is zero for any crossection, x = const of the MEA, i.e.,

$$N = \int_0^{H/2} \sigma_{xx}(x,z)\mathrm{d}z = 0 \tag{31}$$

In case of the closed edges, the resultant force N, defined in (31), cannot be zero, but the overall strain ϵ_x is zero. This will lead to an increase in the contact stress σ_z for all time even in the long term. In fact, in this case, if the plate is flat, and the interface GDL/membrane is impervious, there will be no stress relaxation at all, i.e., the rate of the stress relaxation will be zero.

In the case of the open edges, however, the gel will be capable of deforming laterally, which will lead eventually to its creeping even if the load is transmitted through the flat plates. The rate of the stress relaxation for the case of the flat plates will be much smaller than shown in Figs. 7–9.

7. Conclusion

This study confirmed that under applied compressive strains the contact stress in the membrane electrode assembly (MEA) will drop with time. The maximum contact stress and the rate of stress relaxation depend on the individual properties of the membrane and the gas diffusion layer.

We argued that the rapid and significant stress relaxation of the membrane (gel), during the relaxation test, can be explained by the viscoelastic behavior of membrane's skeleton, in particular, by the small relaxation time and by the large decrease in the modulus of the skeleton with time. The relaxation tests performed for the entire membrane electrode assembly suggested also that the permeability of the membrane's skeleton to fluid motion should be sufficiently low. In addition, these tests suggested that the GDL/membrane interface should be rather impermeable to prevent the liquid flow across the interface.

The gas diffusion layer can be modeled as nonlinear elastic solid with the Mullins effect, i.e., with different elastic modulus during loading and subsequent unloading/reloading. Given that the permeability of the membrane's skeleton is low enough and the interface is rather impermeable, the stress relaxation of the MEA in the short term can be attributed to the rapid decrease in the elastic moduli of the gas diffusion layer upon unloading.

The rate of stress relaxation in the long term and the ultimate value of the contact stress in the MEA will depend both on the viscoelastic properties of the membrane and the unloading modulus of the GDL at small strains. In particular, significant stress relaxation during the gel compression test explains why the ultimate value of the average contact stress in the MEA is so low.

The maximum value of the average contact stress in the MEA depends on the elastic modulus of the GDL during loading. The higher the modulus of the GDL during loading, the higher the contact stress. In addition, the maximum contact stress depends on the properties of the membrane, in particular, the membrane's initial saturation. If the membrane is initially totally saturated, the contact stress is higher than the experimental value. The assumption that the saturation of the membrane changes from 0.9 to 1 during the loading of the MEA helps to decrease the contact stress and obtain a better match with the experimental results.

We note also that decreasing the period in the location of the channels/lands decreases the rate of the stress relaxation of the MEA. In particular, for the flat plate the rate of the stress relaxation will be very low. However, the ultimate value of the contact stress will be independent of the period.

Acknowledgement

References

ABAQUS, Version 6.2. Hibbit, Karlsson and Sorenson, Inc., Pawtucket, RI.
Biot, M., 1941. General theory of three-dimensional consolidation. Journal of Applied Physics 12, 155–164.
Booker, J.R., Small, J.C., 1987. A Method of computing the consolidation behavior of layered soils using direct numerical inversion of Laplace transforms. International Journal for Numerical and Analytical Methods in Geomechanics 11, 363–380.

Coussy, Olivier, 2004. Poromechanics. Wiley, West Sussex, England. p. 125.

Fenton/Kunz Fuel Cell Research Group, 2003. Design of Gas Diffusion Layer for Hydrogen/Air PEMFCs. Presentation.

Freudenthal, A.M., Spillers, W.R., 1962. Solutions for the infinite layer and the half-space for quasi-static consolidating elastic and viscoelastic media. Journal of Applied Physics 33 (9), 2661–2668.

Guenet, J.M., McKenna, G.B., 1986. The concentration dependence of the compression modulus of isotactic polystyrene/cis-decalin gels. Journal of Polymer Science, Part B (Polymer Physics) 24, 2499–2508.

Ma, H.S., Prevost, J., Scherer, G., 2002. Elasticity of DLCA model gels with loops. International Journal of Solids and Structures 39, 4605–4614.

McKenna, G.B., Guenet, J.M., 1988. The effects of solvent type on the concentration dependence of the compression modulus of thermoreversible isotactic polystyrene gels. Journal of Polymer Science, Part B (Polymer Physics) 26 (2), 267–276.

Rice, J.R., Cleary, M., 1976. Some basic stress diffusion solutions for fluid saturated elastic porous media with compressible constituents. Reviews of Geophysics and Space Physics 14 (2), 227–241.

Scherer, G., 1989. Measurement of permeability. I. Theory. Journal of Non-Crystalline Solids 113 (2–3), 107–118.

Tanaka, T., Hocker, L., Benedek, G., 1973. Spectrum of light scattered from a viscoelastic gel. The Journal of Chemical Physics 59 (9), 5151–5159.

Wolgemuth, C.W., Mogilner, A., Oster, G., 2004. The hydration dynamics of polyelectrolyte gels with applications to cell motility and drug delivery. European Biophysics Journal 33 (2), 146–158.

Zhang, X., Hu, Z., Li, Y., 1998. Rubber elasticity of polyacrylamide gels in high network concentration. Polymer 39, 783–2788.